

# Induced Currents and Electron Counting in Aromatic Boron Wheels: $B_8^{2-}$ and $B_9^-$

Patrick W. Fowler\*<sup>†</sup> and Benjamin R. Gray<sup>‡</sup>

Department of Chemistry, University of Sheffield, Sheffield S3 7HF, U.K., and School of Chemistry, University of Nottingham, University Park, Nottingham NG7 2RD, U.K.

Received December 3, 2006

The newly discovered atom-centered polygonal wheels  $B_8^{2-}$  and  $B_9^-$  are predicted to show ring currents characteristic of aromatic systems. Ipsocentric mapping of induced current density for both molecules attributes a  $\pi$  diatropic current to the four electrons of the doubly degenerate  $\pi$  HOMO and a  $\sigma$  diatropic current to the four electrons of the doubly degenerate  $\sigma$  HOMO, each orbital pair having an available transition to corresponding LUMO orbitals in which the angular node count increases by one. Thus, on the magnetic criterion,  $B_8^{2-}$  and  $B_9^-$  are each both  $\pi$ - and  $\sigma$ -aromatic as a consequence of the nodal properties of the frontier orbitals of the  $\pi$ - and  $\sigma$ -stacks.

## 1. Introduction

Recent work by Zhai et al.<sup>1</sup> has produced experimental and theoretical evidence for stable wheel-like anions made up entirely of boron atoms and consisting of centered 7- and 8-cycles (Figure 1). The octagonal wheel structure for  $B_9^-$  had been predicted earlier by Wang and Schleyer.<sup>2</sup> Evidence from photoelectron spectroscopy<sup>3</sup> indicates survival of the heptagonal  $B_8^{2-}$  wheel as a structural unit in pyramidal  $LiB_8^-$ . Both  $B_9^-$  and  $B_8^{2-}$  have been described as aromatic species. Aromaticity has been ascribed to  $B_8^{2-}$  and  $B_9^-$  species on the grounds of energetics, stability, and electron count.<sup>1</sup> Another frequently applied criterion for aromaticity is magnetic, where aromatic/antiaromatic systems are taken, by definition, to be those that support diatropic/paratropic ring currents.<sup>4,5</sup> Currents in cycles are often inferred from calculations of mean magnetic shielding at various points in space, defining nucleus-independent chemical shifts (NICS).<sup>6</sup> In  $B_8^{2-}$  and  $B_9^-$ , although the interpretation is complicated

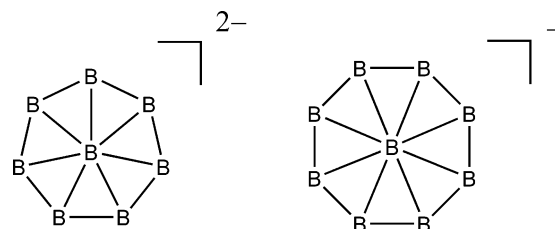


**Figure 1.** Wheel-like structures of the anionic systems  $B_8^{2-}$  and  $B_9^-$ , as proposed in ref 1.

by the fact that the cluster center is occupied by a nucleus, computed negative NICS values over cluster and triangle centers have been taken<sup>1</sup> to indicate ring-current aromaticity for both. Electron counts and the forms of the canonical molecular orbitals were also taken to indicate that the aromaticity had a double  $\sigma + \pi$  character.<sup>1</sup>

A more direct investigation is also possible. Calculation of currents by the ipsocentric<sup>7</sup> method gives information on whether ring current exists, how it compares with the benzene standard of aromaticity, and how it arises from the electronic structure, all predicted from an approach that gives a unique decomposition of induced current into physically separate, nonredundant contributions from occupied orbitals. In this approach, there are simple symmetry-based selection rules for monocycles and similar centered systems:<sup>8</sup> orbital contributions arise from virtual excitations between occupied

\* To whom correspondence should be addressed. E-mail: p.w.fowler@sheffield.ac.uk.

<sup>†</sup> University of Sheffield.

<sup>‡</sup> University of Nottingham.

(1) Zhai, H.-J.; Alexandrova, A. N.; Birch, K. A.; Boldyrev, A. I.; Wang, L.-S. *Angew. Chem. Int. Ed.* **2003**, *42*, 6004.

(2) Wang, Z. X.; von R. Schleyer, P. *Science* **2001**, *292*, 2465.

(3) Alexandrova, A. N.; Zhai, H.-J.; Wang, L.-S.; Boldyrev, A. I. *Inorg. Chem.* **2004**, *43*, 3552.

(4) Pople, J. A. *J. Chem. Phys.* **1956**, *24*, 1111.

(5) Longuet-Higgins, H. C. *Paramagnetic Ring Currents in the [4n]-Annulenes*, in *Aromaticity*; Special Publication No. 21; The Chemical Society: London, 1967.

(6) von R. Schleyer, P.; Maerker, C.; Dransfeld, A.; Jiao, H.; van E. Hommes, N. J. R. *J. Am. Chem. Soc.* **1996**, *118*, 6317.

(7) (a) Keith, T. A.; Bader, R. F. W. *Chem. Phys. Lett.* **1993**, *210*, 223.

(b) Coriani, S.; Lazzeretti, P.; Malagoli, M.; Zanasi, R. *Theoret. Chim. Acta* **1994**, *89*, 181. (c) Steiner, E.; Fowler, P. W. *J. Phys. Chem. A* **2001**, *105*, 9553.

(8) Steiner, E.; Fowler, P. W. *Chem. Commun.* **2001**, 2220.

and unoccupied orbitals, those allowed by in-plane translational symmetry giving a contribution that is diatropic in sense, and those allowed by axial rotational symmetry giving a contribution that is paratropic in sense. Contributions to current are affected by energy differences and spatial distributions, but their global sense is determined by symmetry, angular momentum character, and ultimately nodal count. In these terms, excitations that add exactly one angular node give diatropic currents, whereas those preserving the number of angular nodes give paratropic currents.<sup>8</sup>

In the following sections we calculate the electronic structures of the two closed-shell systems  $B_9^-$  and  $B_8^{2-}$  (Section 2) and give a symmetry analysis (Section 3). Subsequent sections then present current-density maps of the response to a perpendicular magnetic field (Section 4) and show that both exhibit classic perimeter ring currents, which are attributable to the least bound  $\sigma$  and  $\pi$  electrons and intrinsically delocalised in character (Section 5). The orbital model is then used to make predictions for currents in related open-shell systems (Section 6). The main conclusion of the paper (Section 7) is that  $B_9^-$  and  $B_8^{2-}$  are both aromatic on the magnetic criterion.

## 2. Calculations

Optimization at the RHF/6-31G\*\* level yielded centered structures of  $D_{7h}$  and  $D_{8h}$  symmetry for  $B_8^{2-}$  and  $B_9^-$ , respectively, both confirmed as minima by calculation of the Hessian, and with spoke and rim bondlengths  $R_{\text{spoke}} = 1.78$  ( $B_8^{2-}$ ),  $1.98 \text{ \AA}$  ( $B_9^-$ ),  $R_{\text{rim}} = 1.55$  ( $B_8^{2-}$ ),  $1.52 \text{ \AA}$  ( $B_9^-$ ), all within  $0.01\text{--}0.02 \text{ \AA}$  of reported B3LYP/6-311+G\* values.<sup>1</sup> Current density maps were computed<sup>9</sup> at these geometries using the CTOCD-DZ (ipsocentric) method in the same basis. The results are described below and interpreted in terms of the closely similar electronic structures of  $B_9^-$  and  $B_8^{2-}$ .

## 3. Electronic Structure

The occupied bonding orbitals of the boron-wheel molecules arise by interaction of the valence orbitals on the central B atom with the  $\sigma$  and  $\pi$  molecular orbitals of the perimeter atoms. Perimeter  $\sigma$  orbitals can be partitioned in cylindrical symmetry into radial and tangential sets, and as in the Tensor Surface Harmonic theory of 3D clusters,<sup>10</sup> give rise to bonding orbitals through interaction of these two near-equisymmetric manifolds. We will refer to the highest occupied (lowest unoccupied) orbitals of  $\sigma$  and  $\pi$  symmetry as  $\sigma\text{-HOMO}/\pi\text{-HOMO}$  ( $\sigma\text{-LUMO}/\pi\text{-LUMO}$ ). Character tables for the relevant point groups are given by Altmann and Herzog.<sup>11</sup>

**$B_9^-$ .** In  $D_{8h}$  symmetry, a central s orbital has representation  $\Gamma_0 = a_{1g}$  and a central set of p orbitals spans  $\Gamma_{xyz} = a_{2u} + e_{1u}$ . The sets of radial,  $\pi$ , and tangential orbitals on the cycle of eight boron centers span (listed in order of decreasing intrinsic edge-bonding character, and making allowance for

the inverted/Möbius nature<sup>12</sup> of the manifold of tangential orbitals):

$$\Gamma_{\text{radial}}(8) = \Gamma_{\sigma}(8) = a_{1g} + e_{1u} + e_{2g} + e_{3u} + b_{1g}$$

$$\Gamma_{\pi}(8) = \Gamma_{\sigma}(8) \times \Gamma_z = a_{2u} + e_{1g} + e_{2u} + e_{3g} + b_{2u}$$

$$\Gamma_{\text{tangent}}(8) = \Gamma_{\sigma}(8) \times \Gamma_z \times \Gamma_{\epsilon} = b_{2g} + e_{3u} + e_{2g} + e_{1u} + a_{2g}$$

where  $\Gamma_{\sigma}$  is the permutation representation (with character  $\chi(R)$  equal to the number of centers unshifted by operation  $R$ ),  $\Gamma_z$  is the representation of a vector normal to the plane, and  $\Gamma_{\epsilon}$  is the pseudoscalar representation (with  $\chi(R) = +1$  when  $R$  is proper,  $-1$  when  $R$  is improper). In  $D_{8h}$  symmetry,  $\Gamma_z = a_{2u}$  and  $\Gamma_{\epsilon} = a_{1u}$ . The 23 doubly occupied orbitals of  $B_9^-$  span

$$\Gamma_{\text{occ}}(B_9^-) = 4a_{1g} + b_{1g} + b_{2g} + e_{1g} + 2e_{2g} + a_{2u} + 3e_{1u} + 2e_{3u}$$

including 9  $1s^2$  cores, 11  $\sigma$  orbitals formed from bonding combinations of central, tangential and radial orbitals, and 3  $\pi$  orbitals ( $a_{2u} + e_{1g}$ , with 0 and 1 angular nodes, respectively). The  $1s^2$  cores of  $B_9^-$  span  $\Gamma_{\text{core}}(8+1) = \Gamma_0 + \Gamma_{\sigma}(8)$ , and the valence electronic configuration at the RHF/6-31G\*\* level (and at the B3LYP/6-311+G\* level<sup>1</sup>) is

$$3a_{1g}^2(\sigma)2e_{1u}^4(\sigma)2e_{2g}^4(\sigma)2e_{3u}^4(\sigma)4a_{1g}^2(\sigma)1b_{2g}^2(\sigma)1a_{2u}^2(\pi)3e_{1u}^4(\sigma)1e_{1g}^4(\pi)1e_{2u}^0(\pi^*)3e_{2g}^0(\sigma^*)\dots$$

This order is in agreement with Figure 3 of ref 1. The orbital patterns of radial and angular nodes are shown schematically below (in energy order, one representative for each degenerate pair, polygonal icons indicating  $\sigma$  MOs and circular icons  $\pi$  MOs as viewed down the principal axis, a pair of dotted lines separating occupied from unoccupied orbitals).



**$B_8^{2-}$ .** In  $D_{7h}$  symmetry, a central s orbital has representation  $\Gamma_0 = a_1'$  and a central set of p orbitals spans  $\Gamma_{xyz} = a_2'' + e_1'$ . In this group,  $\Gamma_z = a_2''$ ,  $\Gamma_{\epsilon} = a_1''$ . The manifolds of radial,  $\pi$  and tangential orbitals on the perimeter are

$$\Gamma_{\text{radial}}(7) = \Gamma_{\sigma}(7) = a_1' + e_1' + e_2' + e_3'$$

$$\Gamma_{\pi}(7) = \Gamma_{\sigma}(7) \times \Gamma_z = a_2'' + e_1'' + e_2'' + e_3''$$

$$\Gamma_{\text{tangent}}(7) = \Gamma_{\sigma}(7) \times \Gamma_z \times \Gamma_{\epsilon} = e_3' + e_2' + e_1' + a_2''$$

The 21 doubly occupied orbitals of  $B_8^{2-}$  span

$$\Gamma_{\text{occ}}(B_8^{2-}) = 4a_1' + 3e_1' + 2e_2' + 2e_3' + a_2'' + e_1''$$

of which  $\Gamma_{\sigma}(7) + \Gamma_0 = 2a_1' + e_2' + e_3' + e_1''$  is accounted for by B  $1s^2$  cores, so that the valence electronic configura-

(9) Lazzeretti, P.; Zanasi, R. *SYSMO package*; University of Modena: Modena, Italy, 1980. Additional routines, Steiner, E.; Fowler, P. W.; Havenith R. W. A.; Soncini, A.

(10) Stone, A. J. *Mol. Phys.* **1980**, *41*, 1339.

(11) Altmann, S. L.; Herzog, P. *Point-group theory tables*; Clarendon Press: Oxford, 1994.

(12) Fowler, P. W. *Phys. Chem. Chem. Phys.* **2002**, *4*, 2878.

ration at the RHF/6-31G\*\* and B3LYP/6-311+G\* levels is

$$3a_1'^2(\sigma)2e_1'^4(\sigma)2e_2'^4(\sigma)4a_1'^2(\sigma)2e_3'^4(\sigma)1a_2''^2(\pi) \\ 3e_1'^4(\sigma)1e_1''^4(\pi)3e_2'^0(\sigma^*)1e_2''^0(\pi^*)...$$

(again in agreement with Figure 3 of ref 1), with schematic nodal patterns.



As the scheme confirms, the valence configuration of  $B_8^{2-}$  corresponds, apart from minor reordering, to the same angular-momentum progression as for  $B_9^-$ , minus the non-degenerate orbital of highest angular momentum (with four nodes). Of special significance for the orbital interpretation of ipsocentric current-density maps is the fact that, in both  $B_9^-$  and  $B_8^{2-}$ , the lowest-energy transitions of  $\sigma$ - and  $\pi$ -type each increase the number of angular nodes by one. In each system, the  $\sigma$ -HOMO and  $\pi$ -HOMO have angular momentum about the principal axis  $|\Lambda| = 1$ , and the  $\sigma$ -LUMO and  $\pi$ -LUMO have  $|\Lambda| = 2$ . The  $\pi$ - $\pi^*$  transition from the  $e_{1g}/e_1''$   $\pi$ -HOMO pair to the  $e_{2u}/e_2''$   $\pi$ -LUMO pair, and the  $\sigma$ - $\sigma^*$  transition from the  $e_{1u}/e_1'$   $\sigma$ -HOMO pair to the  $e_{2g}/e_2'$   $\sigma$ -LUMO pair are each translationally allowed but rotationally forbidden, indicating purely diatropic contributions to ring current. Since the transitions match in the two molecules, their current-density maps should also match. Strong similarities with the maps for the hypothetical  $CB_6^-$  ion<sup>13,14</sup> are also expected: the valence electronic configuration of

$$3a_{1g}^2(\sigma)2e_{1u}^4(\sigma)2e_{2g}^4(\sigma)1a_{2u}^2(\pi)4a_{1g}^2(\sigma)2b_{1u}^2(\sigma) \\ 3e_{1u}^4(\sigma)1e_{1g}^4(\pi)$$

for this species corresponds to deletion of a  $|\Lambda| = 3$  orbital from the  $B_8^{2-}$  list, and again diatropic  $\pi$  (and  $\sigma$ ) currents arise from HOMO–LUMO transitions within the respective manifolds.<sup>14</sup>

#### 4. Current-Density Maps

Figures 2 and 3 show maps of the current density induced in  $B_9^-$  and  $B_8^{2-}$  by a perpendicular magnetic field, plotted at a height of  $1a_0$  above the plane of the nuclei, and in the case of the  $\sigma$ -HOMO contribution, also in the nuclear plane itself. The maps of total ( $\sigma + \pi$ ) current (a) show a central ring current, with extra features over the nuclear positions. This can be seen to be the sum of (b) a diatropic  $\pi$  ring current (dominated entirely by the contribution of the four  $\pi$ -HOMO electrons), (c) an inner diatropic ring current (the contribution of the four electrons of the  $\sigma$ -HOMO), and (d) a superposition of *paratropic*  $\sigma$  localized circulations, each centered on one of the perimeter nuclei (produced by the  $\sigma$ -complement of the  $\sigma$ -HOMO, i.e., the sum of the all  $\sigma$  orbitals minus the contribution of the  $\sigma$ -HOMO).

(13) Exner, K.; von R. Schleyer, P. *Science* **2000**, *290*, 1937.

(14) Havenith, R. W. A.; Fowler, P. W.; Steiner, E. *Chem.—Eur. J.* **2002**, *8*, 1068.

The maximum value of  $\pi$  current density per unit inducing field at the height of  $1a_0$  is 0.053 au ( $B_9^-$ )/0.050 au ( $B_8^{2-}$ ) (cf. 0.079 in the same units for the  $\pi$  current of benzene in a comparable calculation). At this height above the molecular plane, contributions from core 1s electrons are negligible, and the  $\sigma$  ring current arising from the  $\sigma$ -HOMO pair of orbitals is 0.034 au ( $B_9^-$ )/0.033 au ( $B_8^{2-}$ ), or just under half the benzene standard value. Together, the  $\sigma$  and  $\pi$  ring currents at this height give a total current density per unit of inducing field of 0.099 au ( $B_9^-$ )/0.104 au ( $B_8^{2-}$ ), or 125%/132% of the benzene  $\pi$  current. In the plane of the nuclei (Figures 2e and 3e), the  $\sigma$  ring current arising from the  $\sigma$ -HOMO pair of orbitals is  $\sim 3$  times more intense than in the  $1a_0$  plane.

On the ring-current criterion, both  $B_8^{2-}$  and  $B_9^-$  are aromatic, and they derive this aromaticity from both  $\sigma$  and  $\pi$  systems. Integrated magnetic response properties of these species will therefore have characteristic ring-current contributions. For example, the presence of induced global circulations of both  $\sigma$  and  $\pi$  electrons rationalizes features of the NICS values calculated for these systems in ref 1: their large magnitude, negative sign, and slow decay with height from the molecular plane.

#### 5. Localized Orbital Analysis

The canonical molecular orbitals can be interpreted as combinations of sets of equivalent localized orbitals: for  $B_9^-$ , Pipek–Mezey<sup>15</sup> localization yields nine B 1s cores, eight (bent) two-center BB perimeter bonds, three trigonally directed radial  $\sigma$  orbitals (spanning  $a_{2u} + e_{1g}$ ), and three (also trigonally directed) multi-center  $\pi$  orbitals (spanning  $a_{1g} + e_{1u}$ ). Figure 4 shows the distinct localized orbitals and their individual and collective contributions to the induced current density in the plotting plane  $1a_0$  above that of the nuclei, calculated by the ipsocentric method.<sup>16</sup> The nature of the individual localized-orbital maps, with arrows travelling through the orbital region but not forming cyclic loops of current, illustrates the essentially delocalized nature of both the  $\sigma$  and  $\pi$  electrons of  $B_9^-$ : combination of all three localized  $\pi$  orbitals, and of all three trigonal  $\sigma$  orbitals, is necessary to recover the two ring currents that appear naturally in the treatment on the basis of canonical orbitals. A similar picture is found in the localized treatment of  $B_8^{2-}$ .

#### 6. Aromaticity of Related Species

The anions  $B_9^-$  and  $B_8^{2-}$  are both closed-shell species, and the coupled Hartree–Fock calculations of magnetic response performed here are strictly closed-shell in nature. However, the accompanying orbital analysis can also give a qualitative prediction of the effect on magnetic properties of removal of electrons from the frontier orbitals.

Calculations described in ref 1 predict that the wheel structures of the eight- and nine-boron species survive the loss of one or two electrons.  $B_8$  is predicted to retain full

(15) Pipek J.; Mezey, P. G. *J. Chem. Phys.* **1989**, *90*, 4916.

(16) Steiner, E.; Fowler P. W.; Havenith, R. W. A. *J. Phys. Chem. A* **2002**, *106*, 7048.

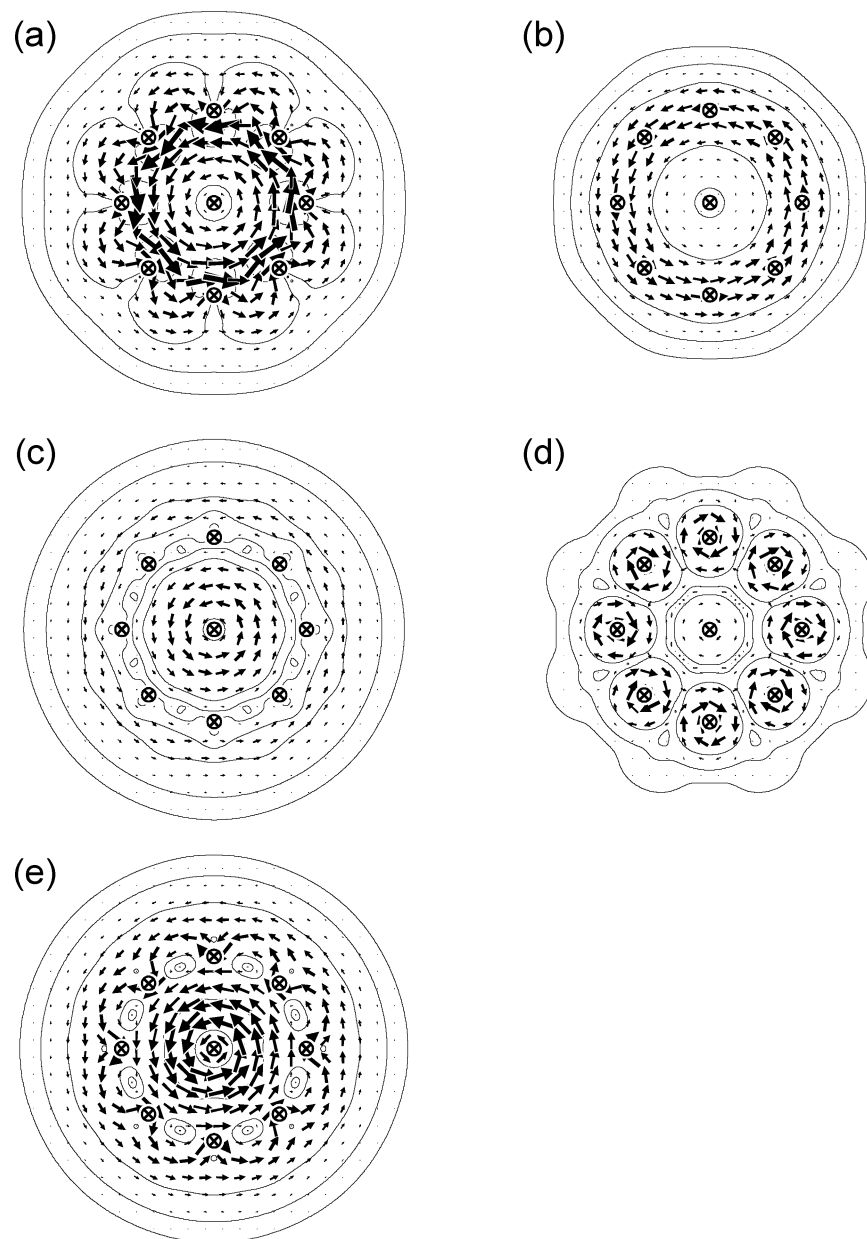


**Figure 2.** Maps of current density induced in  $B_9^-$  by a perpendicular magnetic field. Induced current density is calculated at the ipsocentric CTCD-DZ/6-31G\*\*/RHF/6-31G\*\* level. The separate plots show the contributions from (a) all ( $\sigma + \pi$ ) orbitals, (b)  $\pi$ -HOMO, (c)  $\sigma$ -HOMO, (d)  $\sigma$ -complement of the  $\sigma$ -HOMO, all plotted in a plane at a height of  $1a_0$  above the nuclei, and for comparison, (e) the  $\sigma$ -HOMO contribution to current plotted in the nuclear plane. Plotting conventions: contours represent the magnitude of induced current density per unit inducing field, and arrows its projection in the plotting plane. Counterclockwise circulation of the arrows corresponds to diamagnetic/diatropic current and clockwise circulation to paramagnetic/paratropic current. See text for magnitudes in the separate component maps.

$D_{7h}$  symmetry in the triplet ground state of the  $(1e_1'')^4$  configuration resulting from loss of two electrons from the  $\pi$  HOMO of  $B_8^{2-}$ .  $B_8^-$  also retains a planar wheel-like geometry, with a small  $C_{2v}$ -symmetric in-plane distortion in the doublet ground state of the  $(1a_2)^2(2b_1)^1$  configuration that results from (a) loss of a  $\pi$  HOMO electron of  $B_8^{2-}$  and (b) Jahn–Teller splitting  $e_1'' \rightarrow a_2 + b_1$ . The geometry of  $B_9$  is similarly derived by a  $D_{2h}$ -symmetric distortion of the planar  $B_9^-$  wheel.

High-spin open-shell species have both first- and second-order terms in their energies of interaction with an external magnetic field, raising difficulties for the experimental observation of ring-current effects. With this caveat in mind, the ring currents for  $(e_1'')^4 B_8^{2-}$  and  $(e_1'')^2 B_8$  are expected

to be similar. The analysis parallels that for  $4n\pi$  triplet states of monocycles.<sup>17</sup> Within the  $\pi$  manifold, HOMO–LUMO virtual excitations are allowed under the translational selection rule in both species: in  $B_8^{2-}$  this  $\pi$ – $\pi^*$  excitation is available to four electrons, and in  $B_8$  to only two, but  $B_8$  has an additional excitation channel from the  $1a_2''$  orbital, opened up by the presence of two holes in the  $1e_1''$  HOMO, also contributing diatropic current. The two species have the same  $\sigma$  configuration and should show similar  $\sigma$  ring currents. Thus, in line with long-standing ideas of triplet aromaticity for  $4n\pi$  triplet states of monocycles,<sup>18,1</sup> the ipsocentric method predicts  $4\sigma, 3\pi$  aromaticity for triplet  $B_8$ .

(17) Fowler, P. W.; Steiner E.; Jenneskens, L. W. *Chem. Phys. Lett.* **2003**, *371*, 719.

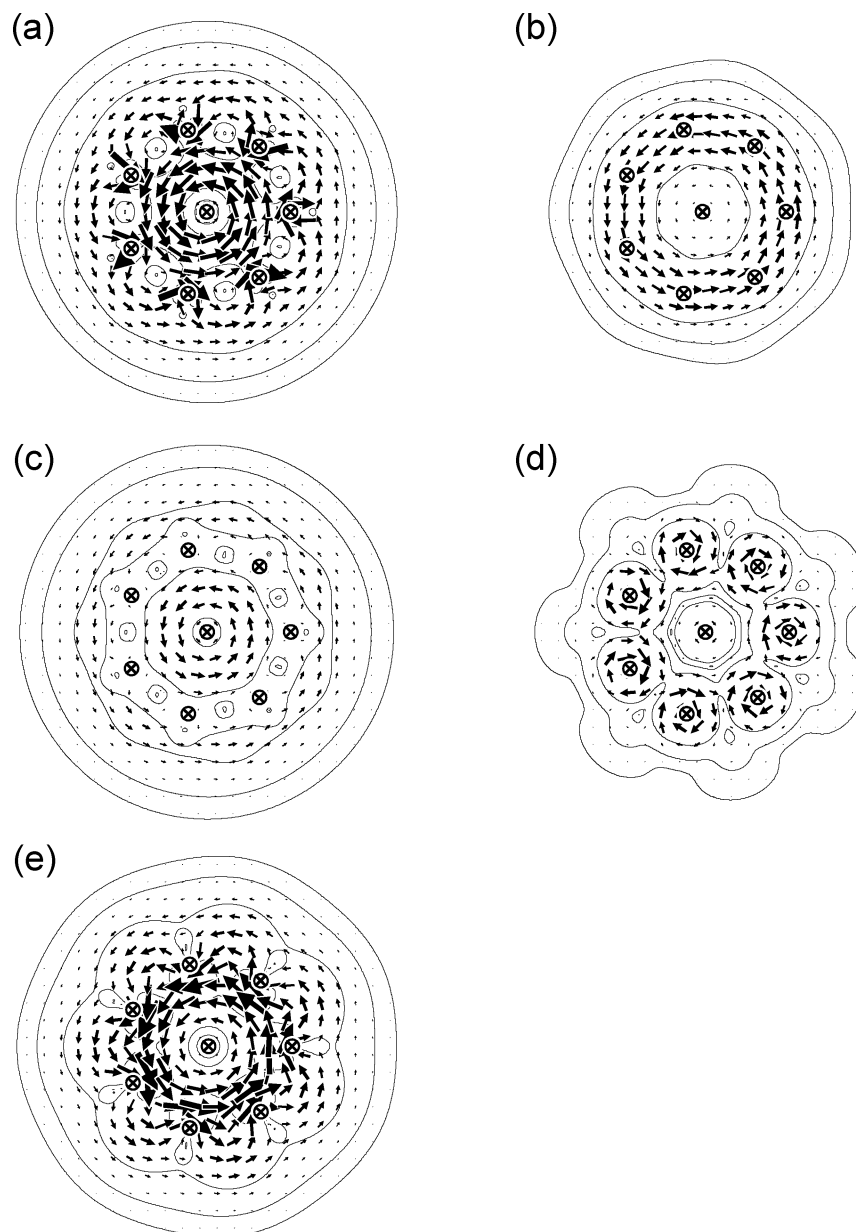


**Figure 3.** Maps of current density induced in  $B_8^{2-}$  by a perpendicular magnetic field. Induced current density is calculated at the ipsocentric CTCD-DZ/6-31G\*\*/RHF/6-31G\*\* level. The separate plots show the contributions from (a) all ( $\sigma + \pi$ ) orbitals, (b)  $\pi$ -HOMO, (c)  $\sigma$ -HOMO, (d)  $\sigma$ -complement of the  $\sigma$ -HOMO, all plotted in a plane at a height of  $1a_0$  above the nuclei, and for comparison, (e) the  $\sigma$ -HOMO contribution to current plotted in the nuclear plane. Plotting conventions as in Figure 2.

Qualitative prediction of the ring currents in the  $B_8^-$  species is complicated by the double effect of the Jahn–Teller distortion in the ground state. On the one hand, the descent in symmetry from  $D_{7h}$  to  $C_{2v}$  gives a formal relaxation of the selection rules, and on the other, it is accompanied by a splitting in the energies of the former HOMO orbitals. If we assume that the basic shapes and nodal properties of the orbitals are unchanged, the contributions of virtual excitations from  $a_2 + b_1 \pi$  ‘HOMO’ to the  $a_2 + b_1 \pi$  ‘LUMO’, and from the  $b_1 \pi$  ‘HOMO-1’ to the  $b_1$  component of the  $\pi$  ‘HOMO’ all remain diatropic. However, as the formerly degenerate ‘HOMO’ is now Jahn–Teller split into  $a_2$  and  $b_1$  components, there is a new channel: the (spin-conserving) virtual excitation of a  $b_1$  ‘HOMO’ electron into

the hole in the  $a_2$  ‘HOMO’. This is an excitation between rotationally matched orbitals with equal numbers of angular nodes (in this case, one), and so contributes a paratropic current. Moreover, the gap in energy between the participating orbitals originates from Jahn–Teller distortion and so should be ‘small’, and perturbation theory<sup>7c</sup> predicts that this will be an intense current. Without a detailed treatment using an as-yet unavailable open-shell ipsocentric procedure, it is impossible to be certain, but it seems likely that the paratropic term will at least cancel the diatropic contributions, leading to a picture of  $B_8^-$  as  $\sigma$ -aromatic but  $\pi$ -non- or anti-aromatic.

## 7. Conclusion

Calculations of induced current have been used to construct maps of the ring currents in two boron-wheel systems. The conclusion, on the magnetic criterion of aromaticity, is that

(18) Baird, N. C. *J. Am. Chem. Soc.* **1972**, *94*, 4941.

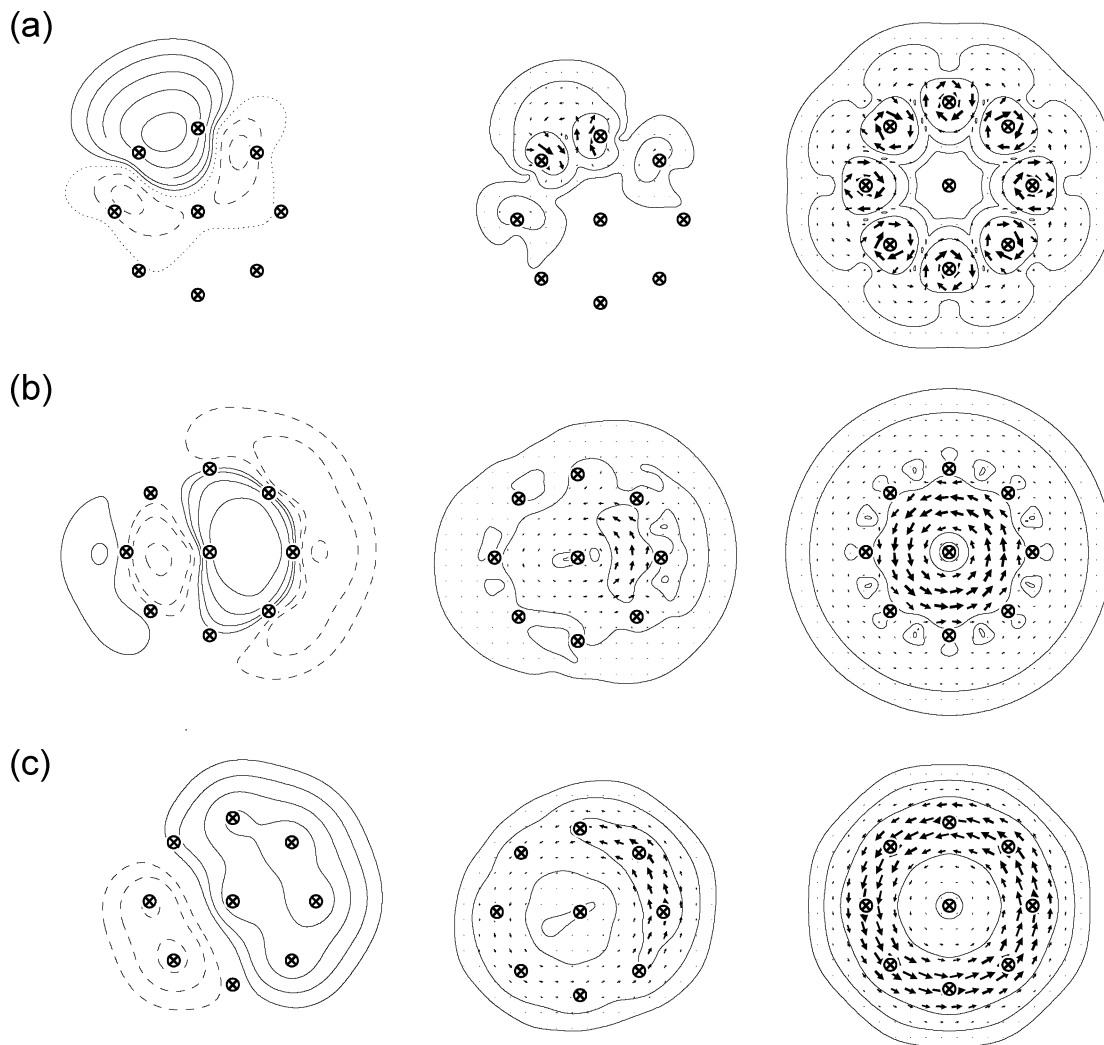


**Figure 4.** Contributions of localized orbitals to the current density induced in  $B_9^-$  by a perpendicular magnetic field. Induced current density is calculated at the ipsocentric CTOCD-DZ/6-31G\*\*/RHF/6-31G\*\* level and coanonical orbitals are localized using the Pipek–Mezey procedure. The three rows of plots show one example from a set of equivalent localized orbitals, the contribution current density arising from that orbital, and the total current density arising from the full set of equivalent orbitals. The rows illustrate orbitals and current maps for (a) localized B lone pair, (b) B–B bonding, and (c) the  $\pi$  orbitals of  $B_9^-$ . All are plotted in the  $1a_0$  plane. Other plotting conventions are as in Figure 2.

$B_8^{2-}$  and  $B_9^-$  are  $\sigma$  aromatic, with four active  $\sigma$  electrons, and they are also  $\pi$  aromatic, with four active  $\pi$  electrons. This concurs with the conclusion of double ( $\sigma + \pi$ ) aromaticity from electron counting,<sup>1</sup> since both  $\pi$  and  $\sigma$  systems have  $4n + 2$  electron counts (each molecule has three occupied  $\pi$  orbitals and also three occupied  $\sigma$  orbitals describing bonding of the central atom to the perimeter ring). However, the pictures arising from current mapping and electron counting are quite different. Hückel ( $4n + 2$ ) counting, properly speaking applies only to a monocycle and not to any other topology, gives equal weight to all electrons/orbitals; the ipsocentric picture for a monocycle attributes current to four HOMO electrons, as only these electrons are in orbitals with a channel open for virtual excitation under the selection rules. More generally, systems with ‘aromatic’ ( $4n + 2$ ) $\pi$  electron counts but without substantial  $\pi$  ring current are known, as are aromatic systems with ‘antiaro-

matic’  $4n\pi$  electron counts and vice versa (phenalene cation and anion both support diatropic perimeter  $\pi$  ring currents, but azaphenalene has a paratropic  $\pi$  ring current;<sup>19</sup>  $Al_4^{2-}$  has two  $\pi$  electrons but no substantial  $\pi$  ring current<sup>20</sup>). The ipsocentric approach to magnetic response tells us for all these systems and for the boron wheels that it is not the number of electrons but the nodal properties and energies of the frontier orbitals that count for the aromaticity of a delocalized system.

**Acknowledgment.** P.W.F. thanks the Royal Society/Wolfson Scheme for a Research Merit Award.

IC062302T

- (19) Cyrański, M. K.; Havenith, R. W. A.; Dobrowolski, M. A.; Gray, B. R.; Krygowski, T. M.; Fowler P. W.; Jenneskens, L. W. *Chem.–Eur. J.* **2007**, *13*, 2201.  
 (20) Havenith R. W. A.; Fowler, P. W. *Phys. Chem. Chem. Phys.* **2006**, *8*, 3383.